Available online at www.sciencedirect.com
ScienceDirect
Journal of the European Ceramic Society 30 (2010) 3035–3039
www.elsevier.com/locate/jeurceramsoc

Homogeneous doping of ceramics by infiltration–gelation

Lanlin Zhang, Hendrik Verweij *

Group Inorganic Materials Science, Department of Materials Science & Engineering, The Ohio State University, Columbus, OH 43210-1178, USA

Received 16 March 2010; received in revised form 15 June 2010; accepted 2 July 2010
Available online 31 July 2010

Abstract

Advanced ceramics require small amounts of cation dopants to improve the sintering process or achieve certain properties. Dopant precursors are often dissolved in initial processing liquids, which may adversely affect ceramic colloidal stability, and dopant transport during drying. This would lead to chemical and microstructural inhomogeniety in the eventual ceramics. Here we present a method that circumvents these problems using the example of Al^{3+}-doped TiO_2 ceramics. Homogeneous TiO_2 compacts with 34% porosity are first prepared by colloidal casting and calcined at 700 °C. The obtained compacts are infiltrated with an aqueous solution of $Al(NO_3)_3$, citric acid and ethylene glycol. The solution composition is adjusted such that during drying, a gel forms that covers the internal pore surface. Subsequent decomposition of organics results in a homogeneous dopant distribution in the porous and then dense-sintered TiO_2 compacts. This is verified with SEM-EDX, and laser ablation coupled ICP-MS on dense compacts sintered at 1100 °C.

Keywords: Cation doping; Infiltration–gelation doping; Microstructure; TiO_2; Sintering

1. Introduction

Cation doping is widely used in advanced ceramics to improve the sintering process and to achieve required properties. Very well known examples are MgO in dense α-Al_2O_3 to obtain translucency,[1] SiO_2 in low-loss ferrites to obtain a small grain size,[2] and Bi_2O_3 in ZnO to obtain varistor properties.[3] In the case of dense TiO_2, cation dopants are commonly used for the optimization of its electric and photo-catalytic properties.[4–10] The doping methods include solid-state cofiring of dopant oxides,[4,5] mixing dopant solutions with powders,[5,6] freeze-drying of mixed dopant and TiO_2 precursor solutions,[7] coprecipitation, simultaneous hydrothermal, and sol–gel synthesis.[8–10] Infiltration of precursor solutions into "pre-sintered" porous compacts, reported for doping alumina,[11] can also be applied to TiO_2. All these methods have specific merits but inherently interfere with processing and can result in an inhomogeneous dopant distribution in the sintered dense TiO_2. For example, cofiring methods require high sintering temperatures, while for the co-synthesis methods it is difficult to properly adjust the reaction rates of dopants and titania precursors. Solution mixing with TiO_2 powders affects the colloidal stability, while infiltration of simple aqueous or nonaqueous precursor solutions leads to segregation of dopants towards small pores and external surfaces.[12] This is because during falling rate period 1 of drying (FRP1), solutions experience a higher capillary force at smaller pores than bigger ones, and also convection force towards the external surface.

In our studies of low-loss TiO_2 ceramics, we found the doping inhomogeneity was determined by the doping method, and must be avoided to achieve the required low dielectric loss. In addition, such TiO_2 compacts should have a dense structure with homogeneous fine grains and minimal Ti^{4+} reduction.[13] Therefore, a low sintering temperature of 1100 °C was applied, which limited dopant homogenization by diffusion. All these led us to develop a method for a fully homogeneous dopant distribution in the dense-sintered TiO_2, using the following guiding principles:

- Separation of optimized compaction processing from dopant introduction.
- Infiltration, followed by complete immobilization of the dopant.

* Corresponding author at: 2041 N College Road, 291A Watts Hall, Columbus, OH 43210-1178, USA. Tel.: +1 614 247 6987; fax: +1 614 688 4949.
E-mail addresses: Verweij@matsceng.ohio-state.edu, verweij.1@osu.edu (H. Verweij).

0955-2219/$ – see front matter © 2010 Elsevier Ltd. All rights reserved.
doi:10.1016/j.jeurceramsoc.2010.07.009

Homogenous porous TiO_2 compacts are first prepared by colloidal casting of optimized dispersions, followed by pre-sintering at 700 °C for 10 h.[13] This heat treatment condition at 700 °C is the lowest temperature where the pure rutile phase forms, while the compact has a moderate porosity of 34% with a sufficient strength for solution infiltration.[13] The dopant solution is then prepared with citric acid (CA) and ethylene glycol (EG) present, based on the Pechini method.[14] It ensures that a rigid gel is formed from CA and EG at the beginning of FRP1, thus avoiding dopant segregation in smaller pores and external surfaces. Residual water molecules and organic components are afterward gradually removed while the overall gel structure stays in place so that the dopant does not migrate. Since the rigid CA–EG polyester structure can be made for almost any dopant, our method can be applied for all ceramic processes that have a homogeneous porous stage.

2. Experimental procedure

2.1. Porous TiO_2 and infiltration solution

The porous TiO_2 compacts (p-TiO_2) were prepared according to the method described in [13]. TiO_2 powders (Ishihara Corp.) were used as-received, with >99.99% purity and 72.7 wt% rutile phase. The powders were ultrasonically dispersed and colloidally stabilized in $p_H = 10.5$ NH_3 aqueous solution. The suspension was screened with a 10 μm aperture Nylon mesh, and pressure-filtrated to form green disk-shaped compacts. These compacts were calcined at 700 °C in air for 10 h, and also pre-dried at 200 °C before infiltration to remove superficial water.

The infiltration solution was prepared from $Al(NO_3)_3{\cdot}9H_2O$ (99.997%), citric acid (CA, ≥99.5%), ethylene glycol (EG, >99%) and, if used, deionized water made with a Milli-Q® ultrapure water purification system. Before addition of $Al(NO_3)_3$, three different CA–EG compositions were studied with a constant CA/EG molar ratio of 0.7/1. The ratio, rounded-up to 0.7, was chosen such that the molar ratio of –COOH group in CA to –OH group in EG equals to 1 for complete esterification. The compositions are: (CAEG1) aqueous solution of 1.0×10^3 mol/m^3 CA and 1.4×10^3 mol/m^3 EG, (CAEG2) aqueous solution of 3.5×10^3 mol/m^3 CA and 5.0×10^3 mol/m^3 EG, and (CAEG3) nonaqueous mixture of 5.2×10^3 mol/m^3 CA and 7.5×10^3 mol/m^3 EG. CAEG2 was finally selected as the infiltration medium for $Al(NO_3)_3$; this infiltration solutions is further indicated as Al^{3+}-CAEG2. The concentration of Al^{3+} ($c_{Al^{3+}}$) in the Al^{3+}-CAEG2 was calculated from the porosity (ϕ_p) in p-TiO_2 and the target doping concentration (x), i.e. molecular ratio of Al/Ti. In an ideal doping process, the total amount of Al^{3+} in the Al^{3+}-CAEG2 equals that of Al in the dense-sintered structure: $n_{Al^{3+}} = n_{Al}$. Therefore

$$c_{Al^{3+}} = \frac{\rho_{TiO_2}}{M_{TiO_2}} \cdot \frac{1-\phi_p}{\phi_p} . x \ \text{mol/m}^3 \quad (1)$$

where M_{TiO_2} (kg/mol) is the molecular weight and ρ_{TiO_2} (kg/m^3) is the density of rutile TiO_2. Three doping concentrations of 0.3, 0.6, 1.2×10^{-3} (300, 600 and 1200 ppm) were studied, corresponding to $c_{Al^{3+}}$ in CAEG2 being 31.0, 62.0 and 124.0 mol/m^3 respectively. For the sake of comparison, a simple aqueous solution of $Al(NO_3)_3$ was prepared, indicated as Al^{3+}-H_2O, for a target doping concentration of 1.2×10^{-3}.

2.2. Infiltration procedure and thermal treatment

The TiO_2 compacts were brought in contact with the infiltration solution from one side to avoid entrapped air. This treatment was carried out inside a closed container to prevent evaporation at external surfaces. The infiltration was verified to be complete when the actual weight gain equaled to the expected weight gain, which was calculated from the accessible pore volume of p-TiO_2, and the Al^{3+}-CAEG2 density of 1.31×10^3 kg/m^3 or the Al^{3+}-H_2O density of 1.00×10^3 kg/m^3. This revealed a complete infiltration in <1 h with no solution being visible on the external compact surface. The Al^{3+} infiltrated p-TiO_2 was heated at 120 °C overnight (~12 h) using a low heating rate of 0.5 °C/min to avoid boiling. A three-step thermal process was thereafter carried out for organic removal and sintering: 0.2 °C/min heating to 450 °C to gradually remove H_2O and/or CO_x, followed by 5 °C/min heating to 1100 °C for 10 h, and then 5 °C/min cooling.

2.3. Characterization

X-ray diffraction (XRD) was performed on as-received powders and calcined TiO_2 samples, using a Scintag XDS2000 diffractometer with Cu Kα radiation ($\lambda = 1.5406$ Å) with $2\theta = 20° \ldots 80°$. The relative density and porosity of p-TiO_2 was measured using a mercury pyconometer (Model DAB100-1, Porous Materials Inc.). The pore size was characterized with a Micromeritics ASAP 2020, and analyzed using the Barrett–Joiner–Halenda method (BET).[15] The viscosity of CAEG2 was measured using a ball drop viscometer (Gilmont Instrument). The contact angle of CAEG2 on dense-sintered TiO_2,[13] was measured with an EasyDrop Contact Angle Measuring Instrument (Krüss). The actual doping concentration was analyzed using a New Wave™ UP 193 Laser Ablation System coupled with a Thermo Finnigan Element 2 Inductively Coupled Plasma Sector Field Mass Spectrometer (LA-ICP-MS). The cross-section of the Al-doped TiO_2 was first ablated on several locations using a 193 nm laser beam. The ablated sample was evaporated and then condensed into small particles, which were carried by a He stream into the ICP-MS. The ICP torch vaporized and ionized the particles, and the resultant plasma was analyzed for the Al concentration. Scanning electron microscopy (SEM) of the as-formed surface and thermally etched cross-sections was performed using a Field-Emission Environmental SEM Philips XL30 (Eindhoven, the Netherlands). Thermal etching was carried out at 100 °C below the sintering temperature. Energy-dispersive X-ray spectroscopy (EDX) in the same instrument was used to detect larger Al-containing particles on the sample surface, while the bulk Al concentration was below the EDX detection limit.

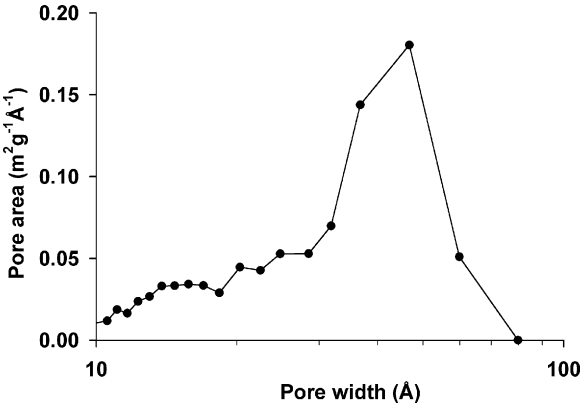

Fig. 1. Pore size distribution in p-TiO_2.

3. Results and discussion

3.1. Porous TiO_2 compact and infiltration

The as-received TiO_2 powders consist of rutile (72.7 wt% from manufacturer data) and next to that, mostly anatase. This was confirmed by XRD. Therefore, the green TiO_2 compacts were first calcined at 700 °C to form 100% rutile and hence avoid interference between the anatase–rutile transformation and the doping process. Complete conversion was also confirmed with XRD. The dominant impurities in the powders were 2.5×10^{-5} Fe_2O_3, 1.0×10^{-5} Nb_2O_5 and 1.0×10^{-5} Na_2O. These concentrations are at least 10 times less than the doping levels used in this study. The p-TiO_2 compact had a porosity (ϕ_p) of 34%, and an average pore diameter of ~45 nm from the BET measurement shown in Fig. 1. The SEM image in Fig. 2 shows the porous and homogeneous microstructure of p-TiO_2.

The gelling temperatures of CAEG1, CAEG2 and CAEG3 solutions were measured to be 110 °C, 120 °C and 160 °C, respectively. This increase was attributed to a decrease in H_3O^+ that catalyzes the gelation. It was found that after gelation, CAEG1, CAEG2 and CAEG3 showed a volume shrinkage of ~70%, ~20% and <5% respectively. The 70% shrinkage for CAEG1 made that the pores were only partially filled with CAEG after drying. On the other hand, the gelled CAEG3 blocked the release of H_2O and CO_x during thermal removal of organics, which led to unacceptable foaming or internal stress. CAEG2 was found to result in a continuous gel structure in the compact after drying without foaming. Therefore it was chosen as a good compromise between shrinkage, and permeability for reaction products during organics removal.

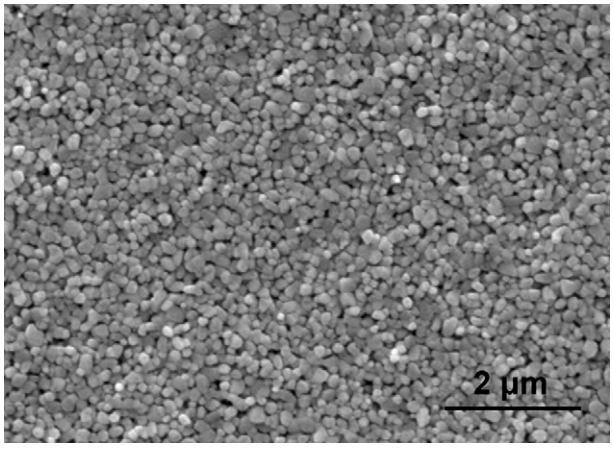

Fig. 2. SEM image of the p-TiO_2 compact surface.

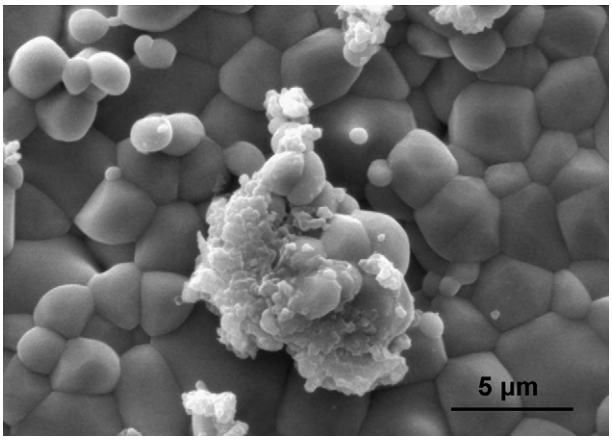

Fig. 3. Al-rich cluster on the surface of 1100 °C sintered TiO_2, prepared from the Al^{3+}-H_2O solution.

The Al^{3+}-CAEG2 solution infiltrated into the p-TiO_2 compact under capillary force. The minimum infiltration time (t^{min}) was estimated from an expression for the liquid propagation rate in a cylindrical channel.[16] Since CAEG2 was found to completely wet TiO_2, this expression was simplified to:

$$\frac{dX}{dt} = \frac{\gamma_{LV} r_p \cos\theta}{4\eta X} \rightarrow t^{min} = \frac{2X^2\eta}{\gamma_{LV} r_p \cos\theta} \quad (2)$$

Table 1
LA-ICP-MS results of the 1100 °C sintered TiO_2, prepared from the Al^{3+}-CAEG2 solution. Sides 1 and 2 are the two sample surfaces.

Target [Al]	[Al] at Side 1	[Al] at Side 2
0.3×10^{-3}	$(0.35 \pm 0.01) \times 10^{-3}$	$(0.35 \pm 0.01) \times 10^{-3}$
0.6×10^{-3}	$(0.65 \pm 0.02) \times 10^{-3}$	$(0.62 \pm 0.02) \times 10^{-3}$
1.2×10^{-3}	$(1.27 \pm 0.02) \times 10^{-3}$	$(1.20 \pm 0.03) \times 10^{-3}$

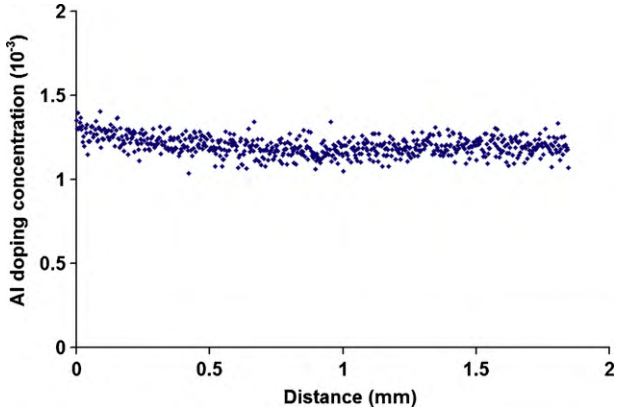

Fig. 4. The Al concentration across the 1100 °C sintered TiO_2, prepared with Al^{3+}-CAEG2 and a target doping of 1.2×10^{-3} Al.

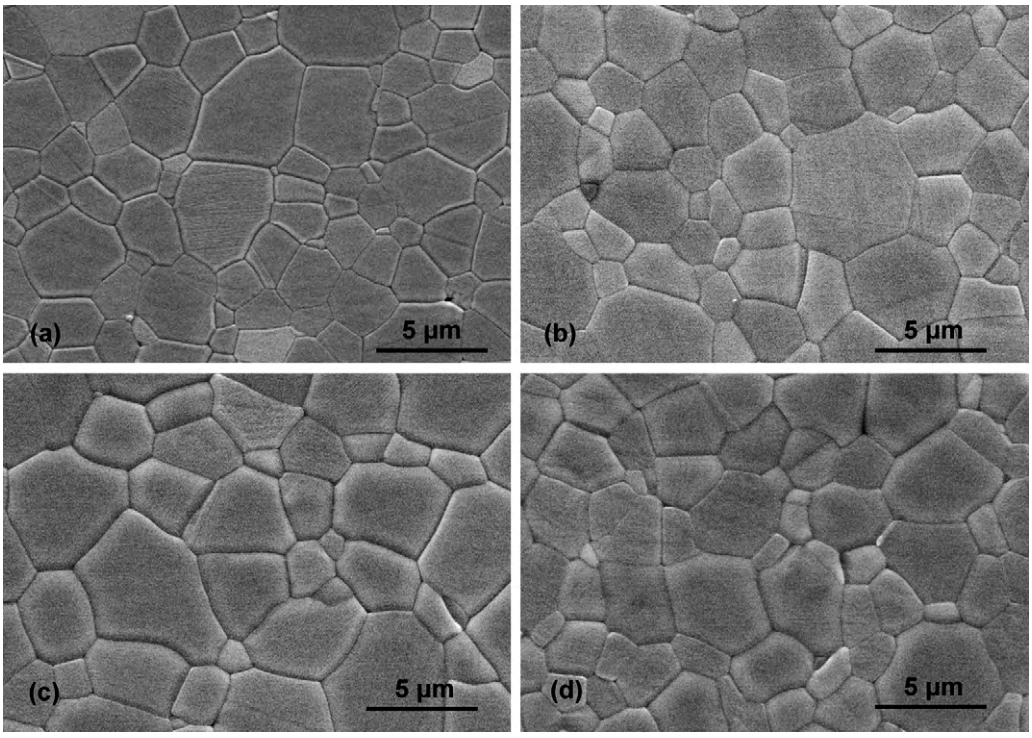

Fig. 5. 1100 °C sintered TiO_2 with (a) no dopant, (b) 0.3×10^{-3} Al, (c) 0.6×10^{-3} Al and (d) 1.2×10^{-3} Al, prepared from Al^{3+}-CAEG2.

where X is the penetration distance, γ_{LV} is the surface tension between the liquid and air, r_p is the channel radius, and η is the liquid dynamic viscosity. X was estimated from the p-TiO_2 compact thickness multiplied by a tortuosity of 3. r_p was taken as 23 nm from Fig. 1. CAEG2 was found to have $\eta = 39.9 \pm 2.0$ mPa s, $\gamma_{LV} = 57.1 \pm 0.4$ mN/m and $\theta = 38.9 \pm 4.6^\circ$ on dense TiO_2, all measured at 20 °C. Substitution of these values into (2) gave an estimated time of 0.8 h for a complete single-sided infiltration of the Al^{3+}-CAEG2 solution in a 2 mm thick p-TiO_2 support. For the Al^{3+}-H_2O solution with $\eta = 1.0$ mPa s at 20 °C, the estimated infiltration time was 0.02 h. As a result, all infiltration treatments were carried out for 1 h to ensure complete penetration for both solutions at 20 °C. After this treatment no solution or precipitation was observed on both p-TiO_2 surfaces, which confirmed our calculation of the required solution volume and the infiltration time.

3.2. Al-doped sintered TiO_2

The three doping concentrations studied here were all below the solubility limit as reported in.[17,18] Al-doped TiO_2, prepared by Al^{3+}-H_2O infiltration, was found to have small Al_2O_3 clusters on the external surface as shown in Fig. 3, and confirmed by EDX analysis. Such clusters were not observed for TiO_2 prepared with Al^{3+}-CAEG2 infiltration. Since the thermal treatment steps was the same for both Al^{3+}-H_2O and Al^{3+}-CAEG2 infiltrations, this shows that the infiltration method played an important role in the final distribution of cation dopants. During gelling and organic removal, there was no coloration or other visible changes in TiO_2 samples. The actual [Al] in 1100 °C dense-sintered TiO_2, was close to the targeted values, as summarized in Table 1. The LA-ICP-MS also revealed homogeneity of Al doping concentration across the sample thickness. An example is shown in Fig. 4 for the sintered TiO_2 with a target doping of 1.2×10^{-3} Al^{3+}. The small systematic deviations between the actual and targeted doping concentrations are ascribed to changes in the $Al(NO_3)_3 \cdot xH_2O$ just before solution preparation. SEM images of Al-doped sintered TiO_2 are shown in Fig. 5. The homogeneous dense microstructure was attributed to both the uniform doping and the homogeneous green compact microstructure.

4. Conclusions

The infiltration–gelation method as presented is found to result in a perfectly homogeneous distribution of Al dopant in TiO_2. Homogeneous and porous TiO_2 compacts were infiltrated with an aqueous solution of $Al(NO_3)_3$, concentrated CA and EG, followed by slow drying and solvent removal to achieve an ultimate homogeneity in dopant distribution. The optimum concentration of CA and EG is obtained as a compromise between gel shrinkage due to water evaporation, and permeability of reaction products during organics removal. As a result, homogeneous dopant distribution was achieved over the internal rigidized gel that gradually decomposes without dopant segregation. The resulting Al-doped sintered TiO_2 revealed a uniform doping profile as opposed to that obtained by aqueous solution infiltration. This method clearly circumvents problems found with process interference and segregation in state of the art methods in.[4–11] We believe our infiltration method is of generic use. The precursor compositions of CA and EG are economically viable for advanced ceramics and allow bulk formulation. Solution optimization is primarily determined by the CA/EG/H_2O ratio, and

easily adapted for any ceramic process. Depending on the actual ceramic process, consolidation and thermal processing can be adjusted to the price/performance target.

Acknowledgement

This work was supported by the U.S. Air Force Office of Scientific Research under the grant #FA9550-04-1-0359.

References

1. Coble R.L. Transparent Alumina, U.S. pattern 3,026,210; 1962.
2. Franken PEC, Doveren HV, Verhoeven JAT. The grain boundary composition of manganese–zinc ferrites with calcium oxide, silicon dioxide, and titanium oxide additions. *Ceram Int* 1977;**3**(3):122–3.
3. Fujitsu S, Toyoda H, Yanagida H. Origin of zinc oxide varistor. *J Am Ceram Soc* 1987;**70**(4). C/71–2.
4. Wang WY, Zhang DF, Xu T, Li XF, Zhou T, Chen XL. Effect of temperature on nonlinear electrical behavior and dielectric properties of (Ca, Ta)-doped TiO_2 ceramics. *Mater Res Bull* 2002;**37**:1197–206.
5. Templeton A, Wang X, Penn SJ, Webb SJ, Cohen LF, Alford NM. Microwave dielectric loss of titanium oxide. *J Am Ceram Soc* 2000;**83**(1): 95–100.
6. Okutan M, Basaran E, Bakan HI, Yakuphanoglu F. AC conductivity and dielectric properties of Co-doped TiO_2. *Physica B* 2005;**364**:300–5.
7. Wang Q, Lian G, Dickey EC. Grain boundary segregation in yttrium-doped polycrystalline TiO_2. *Acta Mater* 2004;**52**(4):809–20.
8. Morris D, Dou Y, Rebane J, Mitchell CEJ, Egdell RG, Law DSL, et al. Photoemission and STM study of the electronic structure of Nb-doped TiO_2. *Phys Rev B* 2000;**61**:13445–57.
9. Sheppard LR, Bak T, Nowotny J. Electrical properties of niobium-doped titanium dioxide. 1. Defect disorder. *J Phys Chem B* 2006;**110**:22447–54.
10. Yin JB, Zhao XP. Preparation and electrorheological activity of mesoporous rare-earth-doped TiO_2. *Chem Mater* 2002;**14**:4633–40.
11. Volceanov E, Volceanov A, Stoleriu Ş. Assessment on mechanical properties controlling of alumina ceramics for harsh service conditions. *J Eur Ceram Soc* 2007;**27**:759–62.
12. Rahaman MN. *Ceramic processing and sintering*. 2nd ed. Marcel Dekker, Inc.; 2003. Chapter 6, p. 413–15, ISSN 0-8247-0988-8.
13. Zhang L, Shqau K, Mumcu G, Yarga S, Sertel K, Volakis JL, et al. Viable route for dense TiO_2 with low microwave dielectric loss. *J Am Ceram Soc* 2010;**93**(4):969–72.
14. Pechini M. U.S. Patent 3,330,697; 1967.
15. Shqau K, Mottern ML, Yu D, Verweij H. Preparation and properties of porous α-Al_2O_3 membrane supports. *J Am Ceram Soc* 2006;**89**(6): 1790–4.
16. Washburn EW. The dynamics of capillary flow. *Phys Rev* 1921;**17**: 273–83.
17. Yan MF, Rhodes WW. Effects of cation contaminants in conductive TiO_2 ceramics. *J Appl Phys* 1982;**53**(12):8809–18.
18. Slepetys RA, Varighan PA. Solid solution of aluminum oxide in rutile titanium dioxide. *J Phys Chem* 1969;**73**:2157–62.